2,3-Diphenyl-2,3-dihydro-4*H*-1,3-thiaza-4-one heterocycles inhibit growth and block completion of cytokinesis in kinetoplastid parasites

Madeline F. Malfara[1], Lee J. Silverberg[2], John DiMaio[3,†], Anthony F. Lagalante[4], Mark A. Olsen[4], Ekaterina Madison[3], and Megan L. Povelones[1]*

[1]Department of Biology or [4]Department of Chemistry, Villanova University, Villanova, PA 19085 USA; [2]Pennsylvania State University, Schuylkill Campus, Schuylkill Haven, PA 17972 USA; [3]Pennsylvania State University, Brandywine Campus, Media, PA 19063 USA

[†]current address, Department of Biology, Temple University, Philadelphia, PA 19122 USA

*corresponding author megan.povelones@villanova.edu

Abstract

Kinetoplastid parasites are model eukaryotes with a complex cell cycle that is highly regulated both spatially and temporally. In addition, diseases caused by these parasites continue to have a significant impact on human and animal health worldwide. While there have been advancements in chemotherapy for these diseases, there is a continual need for an arsenal of compounds that have robust anti-parasite activity with minimal impact on the human host. While investigating a series of 2,3-diphenyl-2,3-dihydro-4*H*-1,3-thiaza-4-one heterocycles with potential activity against these parasites, we found a pyridothiazinone that inhibits growth of the monoxenous parasite *Crithidia fasciculata* and two life cycle stages of *Trypanosoma brucei*. This inhibition is more pronounced in *T. brucei* and is associated with an unusual pre-abscission cell cycle arrest. Exploring the mode of action for these and related compounds in kinetoplastids may provide tools with which to explore cell cycle regulation in these important organisms.

Keywords: *Trypanosoma brucei*; *Crithidia fasciculata*; cell cycle; cytokinesis; mitochondria; pyridothiazinone

Introduction

Kinetoplastid parasites cause several human diseases affecting millions of people worldwide (1). Despite progress in drug development in recent years, there is a continual need for affordable, effective, and efficient drugs to treat these life-threatening diseases.

Human African Trypanosomiasis (HAT), also known as African sleeping sickness, is endemic to sub-Saharan Africa (2). The causative agent of HAT is the kinetoplastid parasite *Trypanosoma brucei. T. brucei* parasites alternate between their mammalian hosts and an insect host and vector, the tsetse fly. Of *T. brucei*'s many developmental forms, two are readily cultured in the laboratory: the long slender bloodstream form (BSF) and the procyclic form (PCF), which replicates *in vivo* in the midgut of the vector. Sleeping sickness is usually fatal if left untreated. Improved treatment regimens, along with increased surveillance and vector control, have dramatically reduced the number of HAT cases in recent years (3). However, with the possibility of drug resistance (4), there is a need for vigilance and a pipeline of additional drug candidates in order to prevent the resurgence of this disease. Further, several species of *Trypanosoma*,

including *T. brucei brucei* and *T. congolense*, cause disease in domesticated cattle, which has a profound economic impact on the region in addition to impacting HAT elimination efforts (5).

Two other diseases caused by kinetoplastids have an even more widespread impact on human health. Leishmaniasis is caused by several species in the *Leishmania* genus and is transmitted by biting sandflies (6). There are as many as 2 million new cases of leishmaniasis every year, with clinical outcomes ranging from disfigurement to death (7). *Trypanosoma cruzi* causes Chagas disease, which is endemic to Latin America and can lead to chronic disease with few treatment options (8). Although human-infective kinetoplastids have distinct life cycles in both their insect and mammalian hosts, kinetoplastid genomes are remarkably similar. This allows for the possibility of shared drug targets based on common biology.

Not all parasitic kinetoplastids infect mammals. Monoxenous kinetoplastids exclusively infect insects, usually in the intestinal tract (9,10). These include the mosquito parasite, *Crithidia fasciculata*, which has been studied for many years as a model kinetoplastid. *C. fasciculata* is morphologically and genetically related to *Leishmania* (11). The ease and affordability of *C. fasciculata in vitro* culture also make it an attractive model for high-throughput screening.

While elucidation of unique features of kinetoplastid biology can reveal new drug targets, kinetoplastids are also useful model organisms, having diverged early in the eukaryotic lineage (12,13). The group is named for the unique organization of their mitochondrial DNA, called kinetoplast DNA or kDNA. The kDNA consists of thousands of topologically interlocked DNA circles all condensed into a disk found adjacent to the basal body of the flagellum (14). The kDNA is single copy, as are a number of other organelles, including the mitochondrion, flagellum, and Golgi apparatus. For this reason, the cell cycle in these organisms must be highly coordinated in order for proper cell division to occur (15). Despite this, some cell cycle checkpoints, notably mitosis to cytokinesis, are missing or differ between different replicative life cycle stages of the parasite (16). Although much work has been done to describe how cytokinesis proceeds in PCF and BSF *T. brucei* (17–19), the mechanism for the final stages of abscission, during which the two daughter cells finally separate, is not known.

Five-, six-, and seven-membered 1,3-thiaza-4-one heterocycles (Fig 1, (20)) are known to have biological activity (21–23) and can inhibit the growth of *T. cruzi* (21,24,25). In this study, we looked at the activity of six 2,3-diphenyl-2,3-dihydro-4*H*-1,3-thiaza-4-ones (Fig 1) which have shown activity against two human pathogenic fungi (26). We have now tested the activity of these compounds against PCF and BSF *T. brucei* as well as the monoxenous parasite *C. fasciculata*. While these compounds inhibited the growth of both species, in *T. brucei* the effect was dramatic enough to arrest cells at a specific point in the cell cycle.

Methods

2.1 Cell Culture

C. fasciculata strain CfC1 were grown in BHI (Sigma) plus 20 μg/ml hemin on an oscillating platform set to ~100 rpm at 27 °C. Cells used for experiments were taken from mid-log phase cultures (range: 1-5 x 10^7 cells/ml). Procyclic form *T. brucei* strain 29-13 (27,28) were grown in SDM-79 media plus 15% FBS and 7.5 μg/ml hemin at 27 °C. Bloodstream form *T. brucei* strain

90-13 were maintained in HMI-9 media supplemented with 15% FBS at 37 °C, 5% CO_2. Cell lines were maintained in the appropriate selecting drugs: 200 μg/ml hygromycin for *C. fasciculata*; 15 μg/ml neomycin, 50 μg/ml hygromycin and 5 μg/ml blasticidin for PCF trypanosomes; and 1 μg/ml neomycin and 5 μg/ml hygromycin for BSF trypanosomes. Experiments were performed on *T. brucei* during mid-log growth (2 x 10^6-1 x 10^7 cells/ml for PCF and 2 x 10^5-1 x 10^6 for BSF). Cell densities were determined by hemocytometer. *T. brucei* cells were counted live, while *C. fasciculata* cells were fixed prior to counting as described (29). For growth curves, cell counts from different treatments were compared to the untreated sample at each time point using a two-way ANOVA with Geisser-Greenhouse correction and Dunnett's multiple comparisons test (GraphPad Prism).

2.2 Plasmids and cell lines

The *C. fasciculata* mitoGFP-expressing cell line has been described (29). Similarly, a PCF *T. brucei* cell line expressing mitochondrial GFP (mitoGFP) was created by PCR amplification of the mitoGFP gene (30) using primers TbmGFPHD3_f (5'-TATAAGCTTTCGCGGGCTGCACG -3') and TbmGFPNheI_r (5'-TATGCAAGCCGCACCTCCCTGCTGTGCC -3')
and cloning it into the pXSGFPBlast (31) vector using HindIII and NheI restriction enzyme sites to create pXSmitoGFPBlast. MluI-linearized construct was introduced into 29-13 cells using the Human T-cell kit from Lonza and a IIb Nucleofector set to program X-014 according to the manufacturer's instructions. After approximately 18 h of recovery, transfected cells were selected using 5 μg/ml blasticidin. Once a stable line was obtained, cells were cloned out by limiting dilution in a 96-well plate (32), and a clonal cell line, TbmitoGFP_E10, was used for this study.

2.3 Cell fixation and imaging

To fix cells for fluorescence microscopy, 5 x 10^6 cells from mid-log cultures were harvested by centrifugation at 1000 rcf for *C. fasciculata* and 800 rcf for *T. brucei* for 5 min. For *C. fasciculata*, cells were stained with MitoTracker Red CMXRos (Invitrogen) as described (29). *T. brucei* PCF cells were treated similarly with a 50 nM prewarmed MitoTracker solution in SDM-79 for 20 min. After staining with MitoTracker, both *C. fasciculata* and PCF *T. brucei* samples were centrifuged as before, washed 1X with PBS and resuspended in PBS at a concentration of 1E7 cells/ml. 500 μl of cell suspension was pipetted onto either charged slides (for experiments shown in Fig 3, 4, 5 and S3) or poly-L-lysine-coated coverslips (for experiments shown in Fig 7, 8, S4 and S5). Cells were allowed to adhere for 10-20 min in a humid chamber. Coverslips were washed with PBS followed by addition of 500 μl of cold 4% paraformaldehyde in PBS. Cells were fixed for 15 min in a humid chamber. BSF *T. brucei* were fixed in solution with 2% paraformaldehyde for 20 min, followed by centrifugation, resuspension in PBS, and adherence to poly-L-lysine-coated coverslips for 35 minutes. Coverslips were then washed 1X briefly and 2X 5 min in PBS. For immunofluorescence experiments, washes following fixation included 0.1M glycine. Cells were permeabilized with 500 μl 0.1% Triton X-100 (*C.f.* and PCF *T.b.*) or 0.1% NP-40 (BSF) in PBS for 5 min, followed by 2, 5 min washes in PBS. Cells were then incubated in blocking solution (1% normal goat serum and 0.1% Triton X-100 in PBS) for 1 hour at room temperature or 4 °C overnight in a humid chamber. Block was removed and the primary monoclonal anti-alpha tubulin antibody (clone B-5-1-2, Sigma) was applied, diluted 1:1000 in blocking solution. Coverslips were incubated in a humid chamber for 1 h at room temperature,

followed by 3 washes in PBST. Goat anti-mouse secondary antibody, coupled to either Alexa 488 or Alexa 555 (Thermo), was diluted 1:1000 in blocking solution and applied to cells for 1 h, followed by 3X 5 min washes in PBST. Finally, cells were stained with 0.2 μg/ml DAPI in PBS for 5 min. Following DAPI staining, slides were washed 1X briefly and 1X for 5 min in PBS and mounted in Vectashield (Vector Laboratories). Wide-field fluorescent imaging was performed either on a Zeiss Axioscope A1 upright LED fluorescence microscope equipped with a Zeiss AxioCam ICm1 camera or an Olympus IX70 with a Leica DFC7000T camera and EZ LAS software. In samples in which the normal arrangement of DAPI-stained organelles was disrupted, maximum intensity Z-projection of 3 focal planes in ImageJ were used to properly categorize cells according to cell cycle stage. Statistics were performed in GraphPad Prism. For cell cycle studies, significance was determined by a two-way no matching ANOVA with simple effect within rows, using one family per row and corrected for multiple comparisons with Dunnett (Fig 5A), or Tukey (Fig 7A/C, S4B, S5A). For morphological quantitation, significance was determined by a one-way no matching ANOVA and corrected for multiple comparisons with Sidak (Fig 7E, 8B, S5C).

2.4 Chemical Synthesis and Treatment

The six 2,3-diphenyl-2,3-dihydro-4*H*-1,3-thiaza-4-ones used in this paper were synthesized as previously described (20). Purity and exact mass of synthesized compounds was determined by LC-PDA and LC-MS. LC-PDA was accomplished on a Shimadzu Prominence LC-20 and exact mass was measured on a SCIEX Exion LC with a SCIEX 5600+ TripleTOF MS. Separation was achieved on an Agilent Infinity LabPoroshell 120 EC-C18 column maintained at 40 °C with a gradient of 90/10 (water/acetonitrile with 0.1% formic acid) ramped from 5/95 over 6 min at a flowrate of 0.5 mL/min. The TOF-MS was scanned over 100-500 Da and calibrated with the SCIEX APCI positive calibrant solution (Part 4460131) prior to accurate mass analysis. Compound exact mass was measured in positive ESI mode with a DP=100 V, CE=10, GAS1=GAS2=60 psi, CUR=30 psi, ISV=5500 V, and source temperature of 450 °C. Purity was determined by peak area integration at 254 nm. For cell culture studies, samples of the six 2,3-diphenyl-2,3-dihydro-4*H*-1,3-thiaza-4-ones were dissolved in sterile DMSO to a final concentration of 10 mg/ml. *C. fasciculata* (wild-type strain CfC1) and *C. fasciculata* and *T. brucei* cells expressing mitoGFP were treated with the indicated concentrations of each drug and monitored for growth by hemocytometer. A no treatment and DMSO vehicle control, equal to the amount of DMSO present in the highest concentration found in the experimental samples, were also tested.

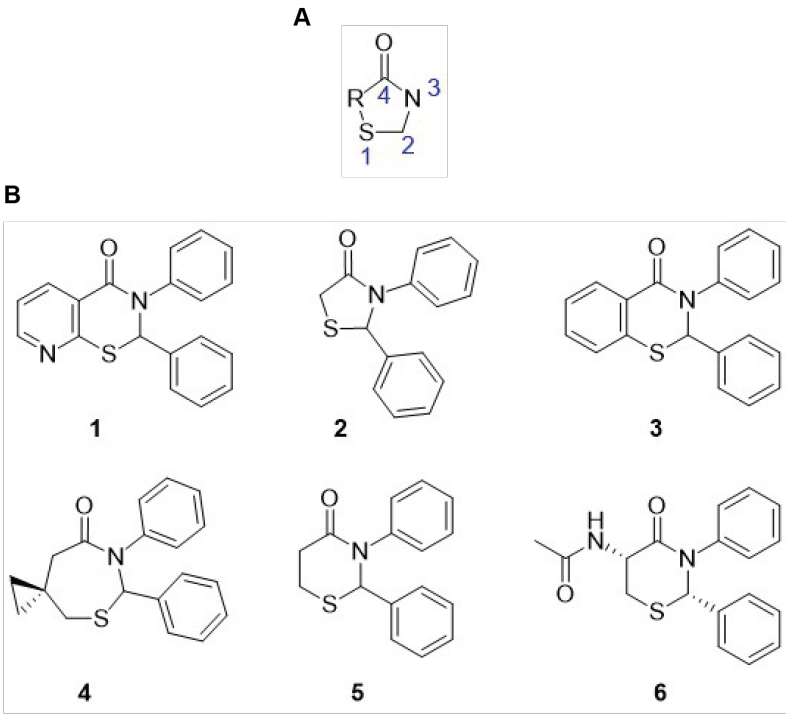

Figure 1. 2,3-diphenyl-2,3-dihydro-4*H*-1,3-thiaza-4-one compounds tested against kinetoplastids. (**A**) Skeleton of the 1,3-thiaza-4-ones. R = a 1, 2, or 3 carbon chain, with or without further substitution. (**B**) Series of specific compounds tested. Synthesis of these compounds was as described (20).

Results and Discussion

To determine if 2,3-diphenyl-2,3-dihydro-4*H*-1,3-thiaza-4-one compounds have biological activity against kinetoplastids, we conducted an initial screen of six compounds (Fig 1) to see how they impacted growth of *C. fasciculata*. We exposed *C. fasciculata* wild-type cells to three different concentrations of each compound during three days of growth and compared cell densities to a culture grown in the presence of the vehicle, DMSO (Fig 2). Compound **1**, a pyridothiazinone, had the most dramatic effect, slowing growth of *C. fasciculata* at all three concentrations, with the greatest effect at the highest concentration of 100 µg/ml. A previous study examining a similar series of compounds showed that 100 µg/ml could inhibit growth of *T. cruzi*, although macrophage cytotoxicity was also observed at this concentration (24). Compound **3**, a benzothiazinone, also slowed growth, although a dose-dependent effect was less apparent. A similar pattern was observed for a thiazolidinone, compound **2**. Two other compounds, a thiazepanone (**4**) and a thiazinone (**5**), showed a minor effect only at the highest concentration, while the last compound, a chiral 5-*N*-acetyl thiazinone (**6**), had no effect on cell growth at any of the concentrations tested. These results could indicate that the addition of the *N*-acetyl group on the 1,3-thiaza-4-one ring effectively eliminates the drug's toxicity; however, we would need to test the activity of the other enantiomer of compound **6** before drawing this conclusion.

Maximal activity was achieved when a fused pyridine or benzene was added, as was the case with compounds **1** and **3**.

To determine the exact mass and purity of our prepared compounds, we performed HPLC separation and detection by PDA and high resolution TOF measurements on an LC-PDA and LC-MS, respectively. All of the compounds were within 1 ppm of the expected masses by high resolution TOF-MS. Purity was calculated from integration at 254 nm and ratioing the compound peak area relative to the total area of all peaks. Results indicate compounds **1**-**6** are 98.9%, 98.0%, 98.2%, 97.4%, 100%, and 95.8% pure, respectively (Fig S1).

Based on the results from our initial growth curves, compounds **1**, **2,** and **3** were chosen for further investigation. *C. fasciculata* cells were treated with 50 µg/ml of each of these compounds in triplicate, and cell density was recorded at 6 time points over the course of 3 days (Fig 3A). Less than 15 hours after the compounds were applied to the cells, a clear difference in cell density was evident. As in our preliminary analysis, compound **1** has the strongest inhibitory effect on cell growth followed by **2** and **3**, respectively. Both the untreated and vehicle controls grew at similar rates.

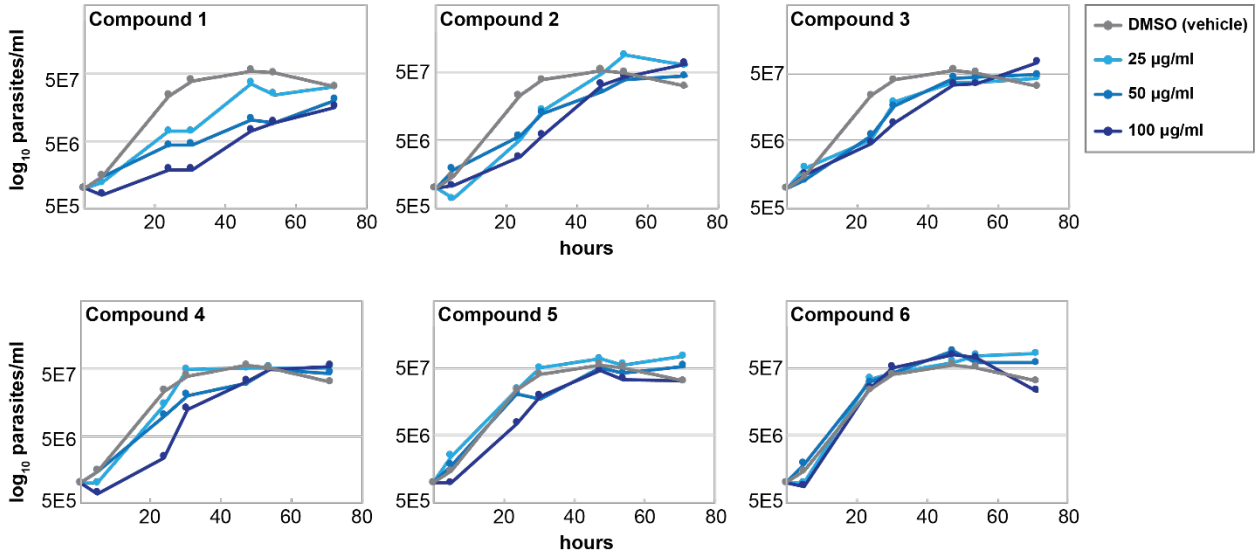

Figure 2. The effect of 2,3-diphenyl-2,3-dihydro-4*H*-1,3-thiaza-4-ones on growth of *C. fasciculata* wild-type strain CfC1. Parasites were grown in the presence of the indicated concentrations of each compound for 72 h. The same DMSO vehicle control is plotted on each graph.

To assess whether treatment with these compounds caused any obvious defects in cell structure and organization, we used fluorescence microscopy. Gross changes in morphology are evident in phase contrast or brightfield microscopy, while disruptions to the cell cycle can be detected by examining the number of DAPI-stained organelles in each cell, including the nucleus and mitochondrial DNA (kDNA). For *C. fasciculata*, in the G1 phase of the cell cycle, there is one nucleus (N) and one kDNA (K) per cell (Fig 3B). As the cell cycle proceeds, nuclear mitosis finishes first, producing 2N1K cells. The kDNA then divides, and cells are referred to as 2N2K. Finally, cytokinesis divides the cell, resulting in two 1N1K daughter cells (29). To provide another marker for cell morphology and metabolic activity, we imaged the mitochondrion.

Kinetoplastid parasites have only a single mitochondrial network per cell which must be faithfully divided during the cell cycle. *C. fasciculata* cells expressing mitochondrial GFP [mitoGFP, (29)] were treated with each compound for up to 72 hours. The impact on growth for each compound was the same as that observed with wild-type cells (Fig S2). MitoGFP can be used to track changes in mitochondrial shape, while MitoTracker Red will only accumulate in mitochondria with a membrane potential.

Despite the effect of these compounds on cell growth, *C. fasciculata* cells treated with 50 µg/ml of compounds **1**, **2**, or **3** displayed no obvious morphological defects, no changes in mitochondrial shape or membrane potential, and no cell cycle arrest that resulted in the clear

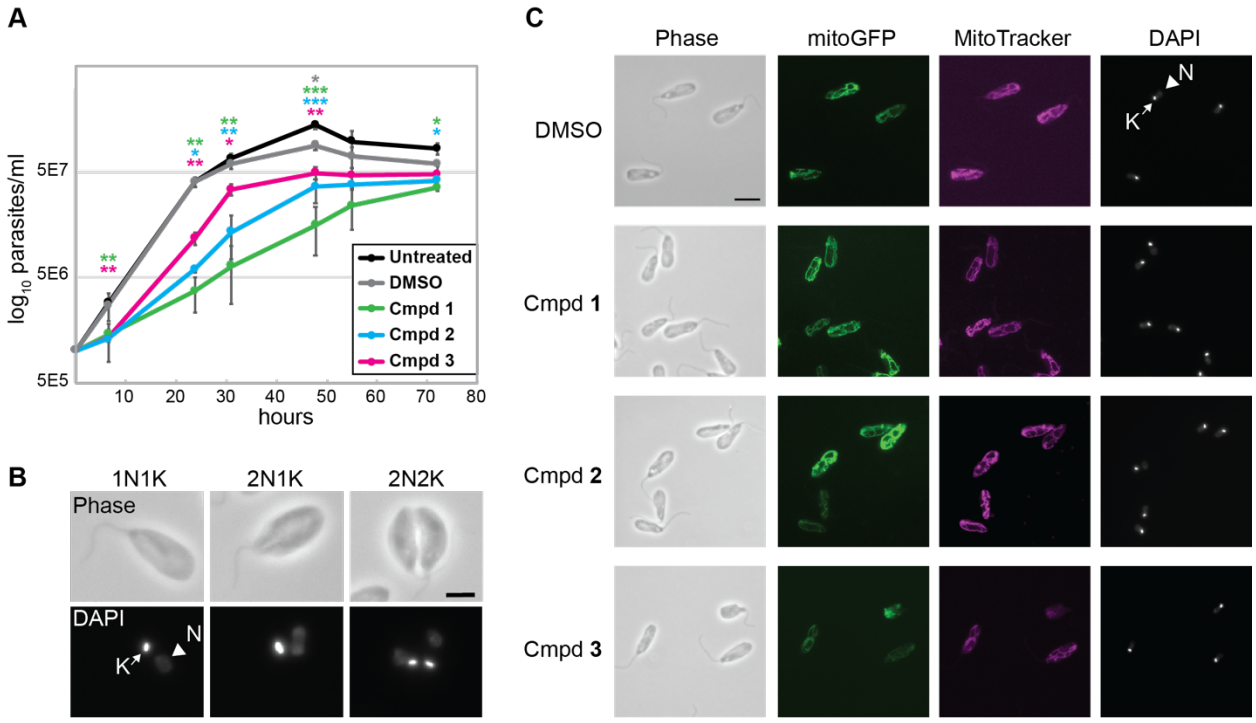

Figure 3. 2,3-diphenyl-2,3-dihydro-4*H*-1,3-thiaza-4-ones inhibit growth of *C. fasciculata* without obvious changes in cell structure or mitochondrial membrane potential. (**A**) The effects of the three most potent inhibitors from previous experiments on the growth of wild-type CfC1 cells were analyzed in triplicate and compared to growth of cells in the presence of the vehicle (DMSO) or cells with no treatment (untreated). Error bars show standard deviation. Significance determined by a two-way ANOVA with a Geisser-Greenhouse correction and Dunnett's multiple comparisons test. Each treatment sample was compared to the untreated sample at each time point. *P<0.05, **P<0.01, ***P<0.001 (**B**) Representative images showing cellular morphology and DAPI staining of *C. fasciculata* cells at different cell cycle stages. N, nucleus, K, kDNA. Scale bar is 2 µm. (**C**) *C. fasciculata* cells modified to express a mitochondrial GFP (mitoGFP) were used to examine mitochondrial structure in the presence of each compound. Cells were also stained with MitoTracker Red (MitoTracker) which accumulates in mitochondria with a membrane potential. Brightly-stained mitochondrial DNA (kDNA) and larger, more faintly-stained nuclei are visible in DAPI staining. All images were taken after 72 h of treatment. Scale bar is 10 µm. Arrow points to kDNA (K); arrowhead points to nucleus (N).

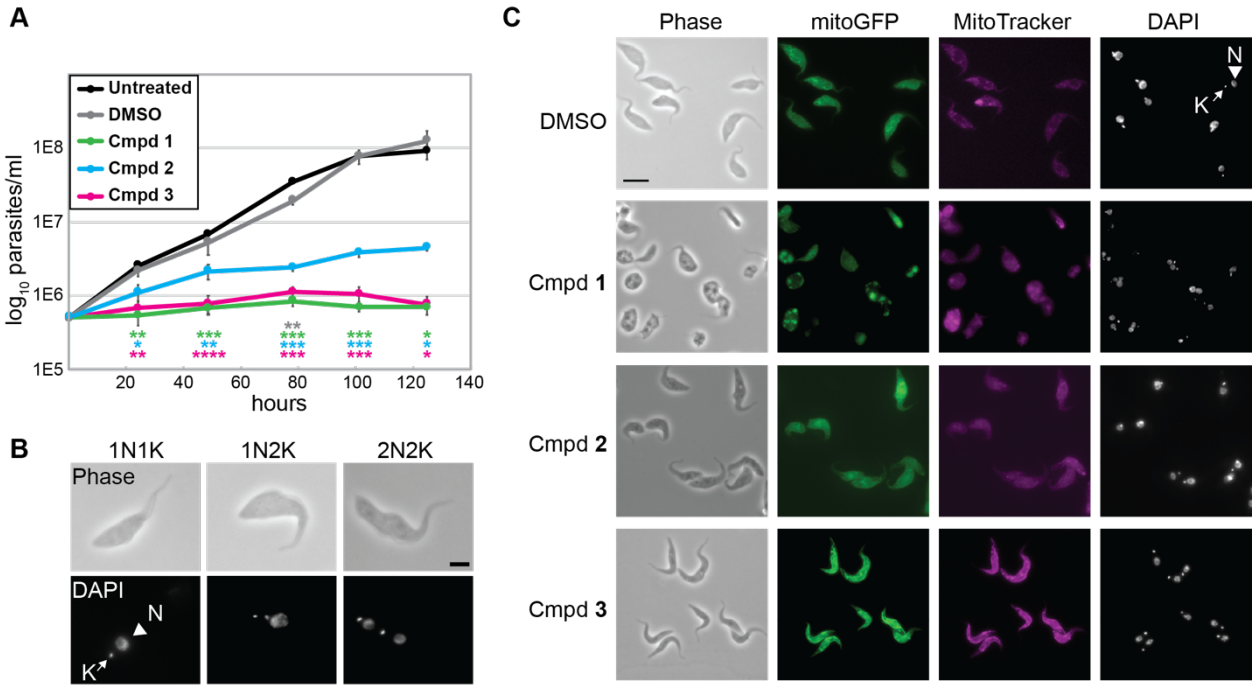

Figure 4. Treatment with 2,3-diphenyl-2,3-dihydro-4*H*-1,3-thiaza-4-ones affects growth and morphology of PCF *T. brucei* expressing mitoGFP. (**A**) Growth in the presence of the indicated compounds (50 µg/ml) or DMSO (vehicle) compared to untreated cells. Cells were diluted when they reached 1 x 10^7 cells/ml and subsequent cell densities were calculated by multiplying the cell density by the dilution factor. Growth curves were performed in triplicate. Error bars show standard deviation. Significance determined by a two-way ANOVA with a Geisser-Greenhouse correction and Dunnett's multiple comparisons test. Each treatment sample was compared to the untreated sample at each time point. *P<0.05, **P<0.01, ***P<0.001, ****P<0.0001 (**B**) Representative images showing cellular morphology and DAPI staining of *T. brucei* cells at different cell cycle stages. N, nucleus; K, kDNA. Scale bar is 2 µm. (**C**) Treated *T. brucei* cells (24 h) were examined by fluorescence microscopy. Cells have been modified to express a mitochondrial GFP (mitoGFP). Cells were also stained with MitoTracker Red (MitoTracker) which accumulates in mitochondria with a membrane potential. Arrow points to mitochondrial DNA (K); arrowhead points to nucleus (N). Scale bar is 10 µm.

accumulation of a particular stage (Fig 3C). Examination of cells after 24 or 48 h of treatment yielded similar results (Fig S3).

We next sought to determine whether these same three 2,3-diphenyl-2,3-dihydro-4*H*-1,3-thiaza-4-ones would inhibit growth of the animal pathogen *T. brucei*. To do this, we treated cultured PCF cells expressing mitoGFP with 50 µg/ml of compounds **1**, **2**, and **3** (Fig 4A). 24 hours after addition of the compounds, treated *T. brucei* cells showed drastically different cell densities than the control samples. Both **1** and **3** inhibited growth almost immediately, while **2** had a more delayed effect. The effect of these compounds on growth was more dramatic than was observed during treatment of *C. fasciculata*. This difference in toxicity between the two species may be

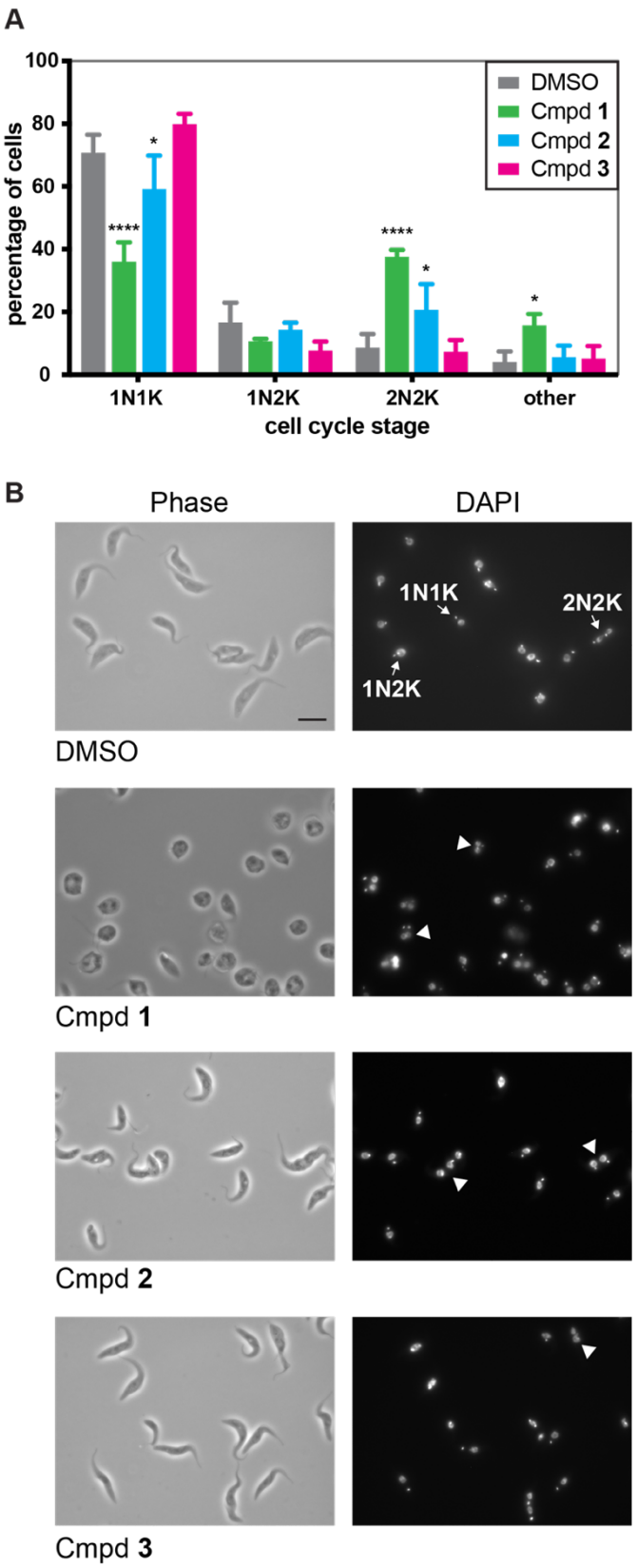

Figure 5. Morphology and cell cycle disruption in PCF *T. brucei* cells treated with 2,3-diphenyl-2,3-dihydro-4*H*-1,3-thiaza-4-ones. (**A**) Quantitation of cell cycle disruption in *T. brucei* PCF cells treated with compounds **1**, **2**, and **3**. Cells were categorized as 1N1K, 1N2K, 2N2K and "other" based on DAPI fields. Abnormal configurations in the "other" category include 2N1K, 0N1K, and cells with more than 2 nuclei and/or kinetoplasts. Microscopy was completed in biological triplicate after 24 h of treatment with 50 µg/ml of the indicated compound or a DMSO vehicle control. For replicate 1, n=26-61 per sample. For replicate 2 and 3, n>200 cells per sample. The same trend was found in each replicate. Asterisks indicate significant differences between treated samples and the DMSO control. * $P<0.05$, **** $P<0.0001$. Significance determined by two-way no-matching ANOVA with Dunnett's correction. (**B**) Representative fields showing *T. brucei* cells treated with each compound. Arrows indicate cells in each cell cycle stage. Arrowheads show 2N2K cells with abnormal arrangements of nuclei and kinetoplasts. Scale bar is 10 µm.

explained by variations in either the molecule bound by these compounds or in the means by which the compounds enter the parasites.

As we did for *C. fasciculata*, we examined treated *T. brucei* cells by fluorescence microscopy (Fig 4B, C). The cell cycle of *T. brucei* differs slightly from that of *C. fasciculata* (Fig 4B). In *T. brucei*, the kinetoplast divides before the nucleus. Cells therefore progress from 1N1K to 1N2K. Nuclear mitosis then creates 2N2K cells before cytokinesis produces two 1N1K cells (16). Cell morphology was dramatically altered in the cells treated with compound **1** (Fig 4C). Cells appeared rounded, possibly indicating a disruption in the overall organization of the cell. We noted that these altered cells usually had

two nuclei and two kinetoplasts (2N2K) or were occasionally multinucleated with multiple kDNA. In many of these cells the mitochondrion is also altered, being condensed into a few bright spots. These bright spots sometimes, but not always, corresponded to MitoTracker signal. This implies that both mitochondrial shape and membrane potential are affected by compound **1**, although from this experiment it was unclear whether this was a secondary effect. In contrast, cells treated with compound **3** showed brighter and more distinct mitochondrial tubules when visualized with MitoTracker.

To quantitate effects on cell cycle progression, we treated *T. brucei* cells with either DMSO (vehicle) or one of the three compounds that inhibited cell growth. We then imaged cells by fluorescence microscopy and categorized them according to the number of DAPI-stained organelles, which is indicative of cell cycle stage (Fig 5). Treatment of *T. brucei* with compound **1** resulted in a clear cell cycle defect, with cells arrested prior to abscission (2N2K). Treatment with compound **2** showed a slight increase in 2N2K cells without noticeable alterations in cell morphology, while compound **3** produced no clear effect on either morphology or cell cycle progression. The accumulation of 2N2K cells indicates that nuclear mitosis and kDNA division are largely unaffected by compound **1**. In addition, a small number of cells (~30% of the "other" category for compound **1**) had more than two nuclei and more than two kinetoplasts, suggesting that some cells are able to re-enter the cell cycle as has been observed with other cytokinesis defects (33,34).

It is possible that these compounds, despite their similarities, interact with different molecular targets. For example, it is possible that the nitrogen in the pyridine ring present in compound **1**, that is absent in compound **3**, interferes with protein function to disrupt the cell cycle, while compounds **2** and **3** interact with different proteins to cause different effects. Alternatively, all three compounds could bind to the same target, but the binding of **1** alters that target's function in a different way, therefore producing a more dramatic phenotype. The slight increase in 2N2K cells following treatment with compound **2** may indicate a common mode of action.

As compound **1** had the most dramatic effect on *T. brucei* cells, we chose this compound for further study. First, we determined the concentration of compound **1** required to inhibit growth to 50% the normal rate (IC50, Fig 6). We grew *T. brucei* PCF and BSF cells in a range of concentrations of compound **1** and determined the percentage of growth inhibition at different time points. For PCF *T. brucei*, the average IC50 was 122.5 μM. For BSF *T. brucei*, the value was somewhat lower, at 86.9 μM. The difference in sensitivity between BSF and PCF *T. brucei* to compound **1** may reflect differences in endocytic rate, and possibly compound uptake, between these life cycle stages. Alternatively, the biological process that is disrupted by compound **1** may be more essential in BSF than in PCF. Although modification of compound **1** may improve its efficacy, these IC50 values are too high for the analyzed compounds to be therapeutically useful. However, we were intrigued by the cell cycle and morphology phenotypes that we observed in both life cycle stages and chose to characterize this further.

In *T. brucei*, an accumulation of 2N2K cells indicates a failure of cells to complete cytokinesis. Regulation of the cell cycle and cytokinesis in these organisms has several unique features (15). Cytokinesis proceeds along the longitudinal axis of the cell, from anterior to posterior, and does not involve a contractile actinomyosin ring (35,36). Cytokinesis in *T. brucei* has four distinct

stages (18). First, an invagination called the division fold appears between the two flagella. This division fold ingresses, eventually forming a gap between the two daughter cells. In late pre-abscission, each daughter cell is clearly defined, but they remain connected by a narrow section of membrane called a "cytoplasmic bridge". Finally, abscission resolves this connection, including cytoskeletal remodeling to create two posterior ends and separation of daughter cells. Determining the target protein or proteins for these compounds might provide insight into the mechanism of cytokinesis in these parasites. Interestingly, recent work to determine the modes of action for current anti-trypanosomal drugs has revealed that suramin, which can be used intravenously to treat stage I HAT, works by inhibiting cytokinesis (37).

PCF cells treated with compound **1** for 24 hours already display a dramatic rearrangement of their cellular morphology. They are rounder than wild-type cells, their mitochondrion appears clumped/collapsed and they are typically at the 2N2K cell cycle stage. This latter finding indicates that either the cell cycle is blocked, which subsequently changes the shape of the cell, or that the cell morphology is disrupted in a way that disrupts the cell cycle. To distinguish between these possibilities, we exposed *T. brucei* cells to 150 µM (47.8 µg/ml) of compound **1** and looked at earlier timepoints to observe the phenotypic progression of treated cells. We also performed immunofluorescence using an anti-alpha tubulin antibody to see if we could detect any gross disruptions in the subpellicular corset of microtubules that determines cell shape. After 12 hours of exposure to compound **1**, 2N2K cells have already begun to accumulate without obvious changes in the intensity or distribution of alpha-tubulin (Fig 7A, B). To further define the exact stage of cell cycle arrest, we sub-categorized 2N2K cells according to the arrangement of nuclei and kinetoplasts (Fig 7C, D). Following nuclear mitosis in PCF cells, this arrangement is typically NKNK (anterior to posterior). As the cleavage furrow continues to separate the two daughter cells, they adopt an NKKN arrangement, in which the divided kDNAs are on either side of the division plane and the cells remain connected for a time by a cytoplasmic bridge (18). In compound **1**-treated PCF cells, we noted an accumulation of NKKN cells at 12 and 24 hours. The prevalence of more unusual DAPI arrangements, such as KKNN (most common in round cells in which cell polarity was disrupted) and KNNK, also increased slightly. After 12 hours of treatment, most 2N2K cells had daughter cell bodies that were elongated rather than round. We

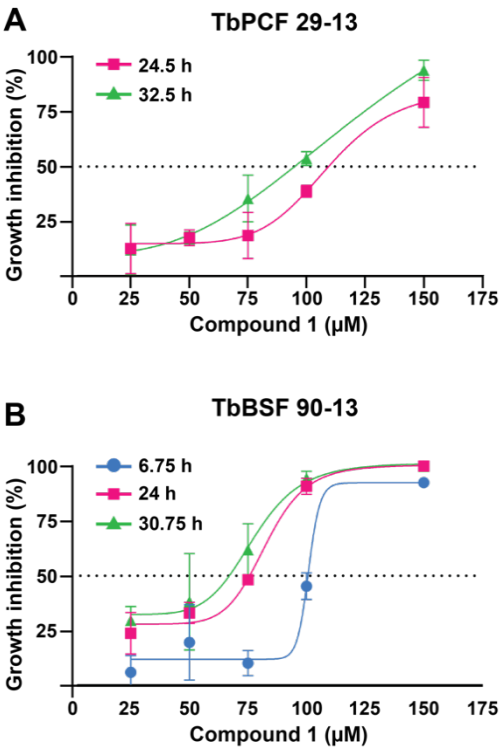

Figure 6. IC50s for compound **1** in both PCF and BSF *T. brucei* cells. (**A**) PCF strain 29-13 or (**B**) BSF strain 90-13 were grown in different concentrations of compound **1**. Cells were counted at 24.5 h and 32.5 h for PCF and 6.75 h, 24 h, and 30.75 h for BSF. The percent of growth inhibition at each time point was calculated by comparing growth of the treated culture to that of a vehicle control (DMSO). For each concentration range, the mean of triplicate experiments is shown. Error bars show standard deviation. Average IC50 across all time points was 122.5 µM for PCF and 86.9 µM for BSF.

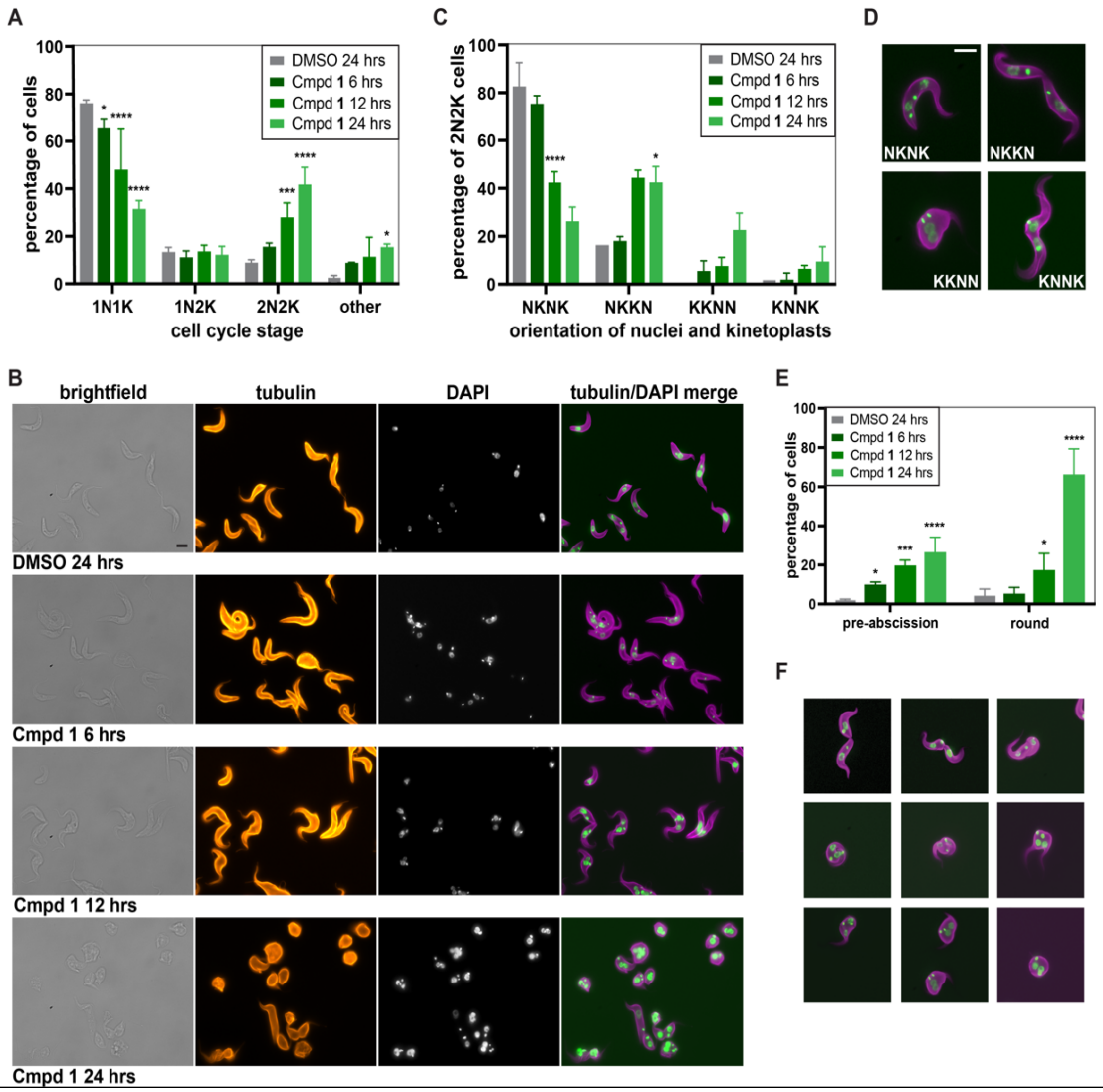

Figure 7. Compound **1** blocks cytokinesis in PCF *T. brucei*. (**A**) Quantitation of cell cycle stages at different times of treatment with 150 µM (47.8 µg/ml) compound **1**. Bars represent the mean of three replicates. Between 100 and 300 cells were counted per sample per replicate. Error bars represent standard deviation. Asterisks indicate significant differences between treated samples compared to the DMSO control at the corresponding time point (note that for simplicity only the final DMSO timepoint is shown on the graph). Significance was determined by two-way no-matching ANOVA with Tukey correction. * P<0.05, *** P<0.005, **** P<0.0001. (**B**) Representative fields of control cells (DMSO) or cells treated with compound **1** for 6, 12 or 24 hours. Tubulin was imaged by immunofluorescence with a mouse anti-alpha tubulin antibody (orange in single channel images). Merged images show tubulin signal in magenta and DAPI in green. Scale bar is 5 µm. (**C**) Subcategorization of 2N2K cells according to the orientation of their nuclei (N) and kinetoplasts (K) from anterior to posterior in cases where cell polarity was maintained. Cells with disrupted polarity were counted, even when anterior and posterior ends could not be distinguished, as was the case for many KKNN cells and some NKNK cells. (**D**) Examples of different 2N2K subtypes. (**E**) Quantitation of pre-abscission cells and cells with a rounded morphology in cultures treated with vehicle or compound **1**. Pre-abscission in this study was defined as cells in mid to late stages of cleavage furrow ingression, with two clearly formed anterior ends. Cells that were pre-abscission but also rounded were included in both categories. (**F**) Examples of cells that may be transitioning from a pre-abscission (top row) to a rounded phenotype (bottom row). Tubulin is shown in magenta and DAPI in green.

also found that a significant portion of NKNK cells in our treated cultures were already in the

mid- to late-stages of cleavage furrow ingression. In DMSO-treated cultures, cells with an advanced cleavage furrow were typically NKKN. To account for this observation, we counted the number of cells, regardless of DAPI arrangement (i.e. NKNK, NKKN, and KNNK), that had a clearly visible cleavage furrow, with well-defined daughter anterior ends, including cells that remained connected by a cytoplasmic bridge. We termed this category pre-abscission, representing the mid to late stages of cleavage furrow ingression up to the point of abscission. After 6 hours of treatment with compound **1**, there is an increase in the number of pre-abscission cells, which increases further at 12 and 24 hours. This indicates that abscission and possibly the rearrangement of DNA-containing organelles may be blocked or slowed in the presence of compound **1** (Fig 7C, D, E). We also counted the number of cells that appeared round rather than elongated in compound **1** versus vehicle-treated cells (Fig 7E). Round cells did not begin to increase until 12 hours of treatment with compound **1** but represent around 50% of the cell population at 24 hours. From this, we conclude that the primary effect of compound **1** treatment is a block in cell cycle progression, with subsequent changes in cell morphology. It is possible that cells begin to become round after being arrested for a period of time, as we occasionally observe pre-abscission cells that appear to be in the process of rounding (Fig 7F).

Although the cell cycles of BSF and PCF cells differ in the arrangement of divided organelles and cell cycle checkpoints (38,39), we also observed an accumulation of 2N2K stages when BSF *T. brucei* were treated with compound **1**. The percentage of 2N2K cells began to increase after 3.5 hours of treatment and increased further at 6 hours (Fig S4A, B). As in our PCF experiments, a number of these cells appear to be at the pre-abscission stage (Fig S4C and S5). We also saw an increase in cells in the "other" category, which includes 1N0K and 0N1K cells but mostly consists of cells with more than 2 nuclei and/or kinetoplasts. This indicates that pre-abscission cells may be able to re-initiate the cell cycle, something that has been demonstrated even for wild-type BSF *T. brucei* (18). In a typical dividing BSF cell, the DAPI-stained organelles have an NNKK arrangement, which we also observed in our control, DMSO-treated cultures (Fig S5A). As in our PCF experiments, treatment of BSF *T. brucei* with compound **1** produced an increase in NKKN cells in as little as 1 hour of treatment (Fig S5A, B). We also observed similar phenotype kinetics, with treated BSF cultures first showing an increase in pre-abscission cells, followed by an increase in rounded cells (Fig S5C, D). Based on the similarities between the BSF and PCF phenotypes in the presence of compound **1**, we surmise that whatever process is being blocked by compound **1** functions similarly in both PCF and BSF. Using RNAi-mediated knockdown, a number of cytokinesis defects have been described in *T. brucei* [reviewed in (19,40,41)]. However, only one protein, a microtubule-severing enzyme called spastin, has been shown definitively to play a role in abscission, and the mutant phenotype was only apparent during spastin knockdown in BSF parasites (42,43). Flagellar motility also contributes to the final stages of cytokinesis, but motility defects produce clumps of multiple partially-divided cells, which we do not observe (44,45). Future work to identify the target of compound **1** might therefore provide mechanistic insights into the mysterious later stages of the cell cycle in *T. brucei*.

The single mitochondrial network in *T. brucei* is a useful landmark for studies of cell morphology. For this reason, our microscopy experiments used a PCF cell line that expresses mitoGFP. Interestingly, we noted that in many of the pre-abscission cells, the daughter cells remained connected by a single mitochondrial tubule in addition to the narrow cytoplasmic

bridge (Fig 8A). It has been suggested that resolution of this final connection between the divided mitochondrial networks is one of the final steps in cell division, immediately preceding or even coupled to cytokinesis (46). In *C. fasciculata*, we have found that these two events, mitochondrial division and cytokinesis, occur nearly simultaneously (29). In *T. brucei*, one study

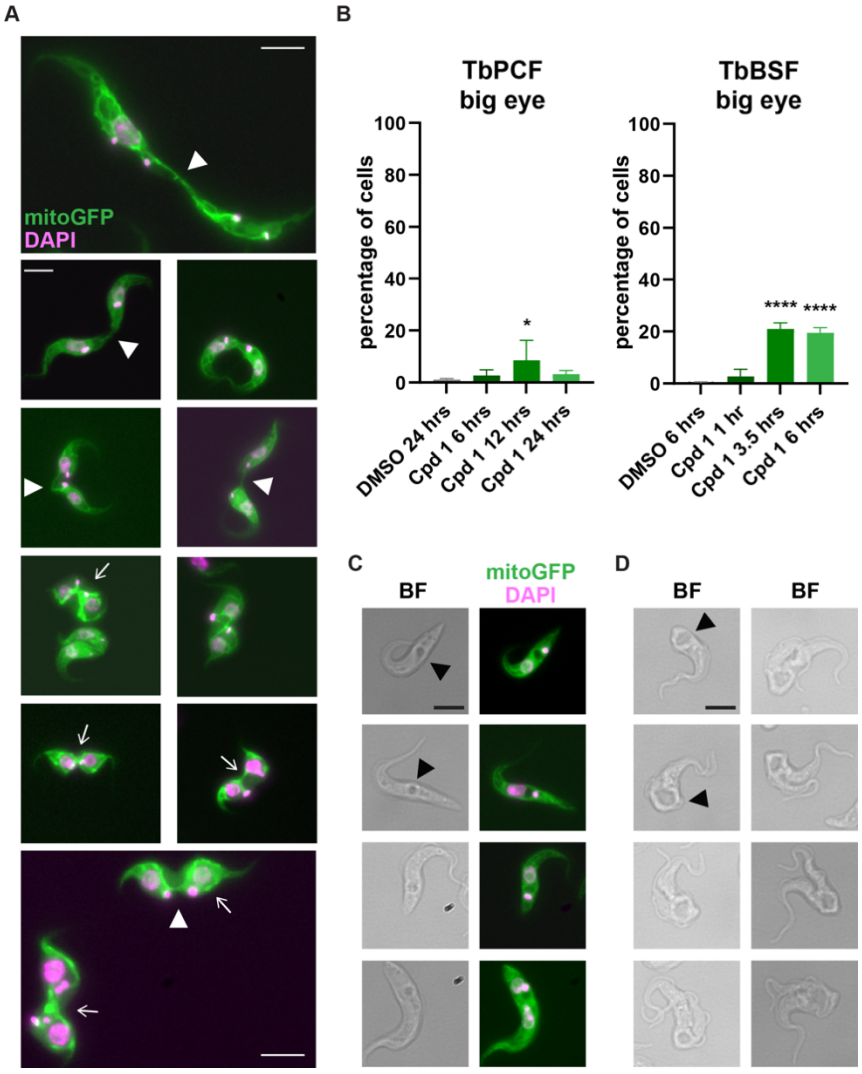

Figure 8. Compound **1** slows mitochondrial division and enlarges the flagellar pocket. (**A**) Examination of pre-abscission PCF *T. brucei* following treatment with compound **1** reveals pre-abscission cells are still linked by mitochondrial tubules. White arrowheads show areas where cells appear to be attached by a single mitochondrial tubule. Arrows indicate cells showing collapsed mitochondrial networks. MitoGFP is shown in green. DAPI is shown in pink. Scale bar is 5 µm. (**B**) Quantitation of cells with an enlarged flagellar pocket ("big-eye") in PCF and BSF *T. brucei* that have been treated with compound **1**. The mean of three replicates is shown. Error bars indicate standard deviation. 100-300 cells were counted per sample per replicate. Asterisks indicate significant differences between treated samples compared to the DMSO control at the corresponding time point (note that only the final DMSO time point is shown on the graph). Significance was determined by one-way no-matching ANOVA with Sidak correction. * P<0.05. ****P<0.0001. (**C**) Examples of PCF cells and (**D**) BSF cells with enlarged flagellar pockets (black arrowheads). In D, the cells shown in the bottom two images of column one and all the cells in column two are what we would call "pre-abscission" due to the presence of two distinct anterior ends as a result of cleavage furrow ingression. Scale bar is 5 µm.

of RNAi-mediated knockdown of the multifunctional dynamin-like protein (TbDLP) reported an accumulation of cells that were blocked in both mitochondrial division and cytokinesis (46). As dynamin-like proteins in other systems mediate mitochondrial division, it was proposed that TbDLP performs this role in *T. brucei*. Further, the authors suggested that knockdown of TbDLP and subsequent inhibition of mitochondrial division trigger a novel cell cycle checkpoint that also blocks cytokinesis, and that this checkpoint is critical to ensure that each daughter cell receives a mitochondrial network.

Other studies that have examined the effects of TbDLP knockdown in *T. brucei* have not observed this defect in cytokinesis, presumably due to differences in RNAi efficiency (47,48). These reports have noted other mitochondrial effects, including "collapse" of the mitochondrial network (47) and increased constrictions along mitochondrial tubules as seen by electron microscopy (47,48). The mitoGFP signal in some of our compound **1**-treated PCF cells appears collapsed, with fewer, thicker mitochondrial tubules (Fig 4C and 8A). This phenotype appears with the same timing as effects on growth and the cell cycle, making it difficult to conclude whether it is a primary or secondary effect of compound **1** treatment. However, many pre-abscission cells retain an apparently normal mitochondrial network (Fig 8), suggesting that the delay in mitochondrial division is not due to a disruption in mitochondrial shape.

To add further complexity, TbDLP-RNAi cells are also defective in endocytosis, leading to the conclusion that *T. brucei*, which lacks genes for classical dynamins, instead has a dynamin-like protein that functions in both endocytosis and mitochondrial division (46,48). Disruption of endocytosis in *T. brucei*, through knockdown of TbDLP, clathrin, or other proteins, causes a characteristic "big-eye" phenotype as a result of enlargement of the flagellar pocket (49).

To see if this aspect of the TbDLP knockdown phenotype was also produced by treatment with compound **1**, we counted the number of cells with an enlarged flagellar pocket at each time point. While the effect is subtle in PCF (Fig 8B, C), there was a distinct accumulation of "big-eye" cells in BSF *T. brucei* cultures treated with compound **1** (Fig 8B, D). The increased penetrance of the "big-eye" phenotype in BSF cells may reflect their enhanced endocytic rate relative to PCF. The similarities between our phenotype and that of TbDLP knockdown cells make TbDLP an intriguing possible target for compound **1** and related compounds. If confirmed by further experimentation, compound **1** may provide a new way to probe the functional complexity of TbDLP and address some of the ambiguities left unresolved by genetic analysis. Alternatively, compound **1** could inhibit the activity of another protein, giving researchers a new tool to explore the connections between endocytosis, mitochondrial division, and the cell cycle in *T. brucei*. For example, it has been proposed that the final event of cytokinesis must involve membrane remodeling or vesicle trafficking to the division plane to mediate membrane fusion (19). The phenotype we describe, which has elements of an endocytosis/vesicle trafficking defect and a cytokinesis defect, may reflect a disruption to this essential process.

The six 2,3-diphenyl-2,3-dihydro-4*H*-1,3-thiaza-4-ones investigated in this study exhibited a range of trypanocidal and cytostatic effects. We focused on the three compounds with the greatest growth inhibition: compounds **1**, **2**, and **3**. As these compounds have been shown to inhibit growth of human pathogenic fungi (26), modifications of these compounds may yet produce good candidates for treatment of trypanosomatid disease. In addition, since treatment

with compound **1** produces an unusual phenotype in *T. brucei*, and overexpression and RNAi-based genetic libraries exist (50,51), trypanosomes would be a good experimental system with which to deduce the molecular target(s) of a therapeutically relevant class of compounds. Such studies are also likely to provide further insight into the unique mechanisms of cell cycle regulation in kinetoplastid parasites.

Acknowledgments
The authors thank Stephen Beverley for the parental CfC1 *Crithidia fasciculata* strain, and Stephen Hajduk for the mitochondrial GFP construct. Thanks also to Lindsay Bair, Laura Anastor-Walters, and Nancy Peltier for technical assistance.

Funding
This work was supported by the National Science Foundation under grant number MCB-1651517 to MLP and by a Major Research Instrumentation Grant to Villanova University (CHE-2018399). LJS was supported by internal funding from Penn State Schuylkill.

References
1. Filardy AA, Guimarães-Pinto K, Nunes MP, Zukeram K, Fliess L, Pereira L, et al. Human Kinetoplastid Protozoan Infections: Where Are We Going Next? Front Immunol. 2018 Jul 25;9:1493.
2. Aksoy S, Buscher P, Lehane M, Solano P, Van Den Abbeele J. Human African trypanosomiasis control: Achievements and challenges. Hotez PJ, editor. PLoS Negl Trop Dis. 2017 Apr 20;11(4):e0005454.
3. Neau P, Hänel H, Lameyre V, Strub-Wourgaft N, Kuykens L. Innovative Partnerships for the Elimination of Human African Trypanosomiasis and the Development of Fexinidazole. Trop Med Infect Dis. 2020 Jan 27;5(1):17.
4. Capela, Moreira, Lopes. An Overview of Drug Resistance in Protozoal Diseases. Int J Mol Sci. 2019 Nov 15;20(22):5748.
5. Simo G, Rayaisse JB. Challenges facing the elimination of sleeping sickness in west and central Africa: sustainable control of animal trypanosomiasis as an indispensable approach to achieve the goal. Parasit Vectors. 2015 Dec;8(1):640.
6. Okwor I, Uzonna J. Social and Economic Burden of Human Leishmaniasis. Am J Trop Med Hyg. 2016 Mar 2;94(3):489–93.
7. Torres-Guerrero E, Quintanilla-Cedillo MR, Ruiz-Esmenjaud J, Arenas R. Leishmaniasis: a review. F1000Research. 2017 May 26;6:750.
8. Pérez-Molina JA, Molina I. Chagas disease. The Lancet. 2018 Jan;391(10115):82–94.
9. Podlipaev SA. Insect trypanosomatids: the need to know more. Mem Inst Oswaldo Cruz. 2000 Aug;95(4):517–22.
10. Wallace FG. The trypanosomatid parasites of insects and arachnids. Exp Parasitol. 1966 Feb 1;18(1):124–93.
11. Opperdoes FR, Butenko A, Flegontov P, Yurchenko V, Lukeš J. Comparative Metabolism of Free-living *Bodo saltans* and Parasitic Trypanosomatids. J Eukaryot Microbiol. 2016;63(5):657–78.
12. Matthews KR. 25 years of African trypanosome research: From description to molecular dissection and new drug discovery. Mol Biochem Parasitol. 2015 Mar 1;200(1):30–40.

13. Hashimi H. A parasite's take on the evolutionary cell biology of MICOS. Read L, editor. PLOS Pathog. 2019 Dec 19;15(12):e1008166.
14. Jensen RE, Englund PT. Network News: The Replication of Kinetoplast DNA. Annu Rev Microbiol. 2012 Oct 13;66(1):473–91.
15. Wheeler RJ, Gull K, Sunter JD. Coordination of the Cell Cycle in Trypanosomes. Annu Rev Microbiol. 2019;73(1):133–54.
16. Ploubidou A, Robinson DR, Docherty RC, Ogbadoyi EO, Gull K. Evidence for novel cell cycle checkpoints in trypanosomes: kinetoplast segregation and cytokinesis in the absence of mitosis. J Cell Sci. 1999 Dec 15;112(24):4641–50.
17. Hilton NA, Sladewski TE, Perry JA, Pataki Z, Sinclair-Davis AN, Muniz RS, et al. Identification of TOEFAZ1-interacting proteins reveals key regulators of *Trypanosoma brucei* cytokinesis: *TOEFAZ1 interactors in* T. brucei. Mol Microbiol. 2018 Aug;109(3):306–26.
18. Wheeler RJ, Scheumann N, Wickstead B, Gull K, Vaughan S. Cytokinesis in *Trypanosoma brucei* differs between bloodstream and tsetse trypomastigote forms: implications for microtubule-based morphogenesis and mutant analysis. Mol Microbiol. 2013;90(6):1339–55.
19. Farr H, Gull K. Cytokinesis in trypanosomes. Cytoskeleton. 2012;69(11):931–41.
20. Silverberg L, Pacheco C, Lagalante A, Cannon K, Bachert J, Xie Y, et al. Synthesis and Spectroscopic Properties of 2,3-Diphenyl-1,3-thiaza-4-one Heterocycles. Int J Chem. 2015 Oct 16;7(2): p150-162.
21. Jain AK, Vaidya A, Ravichandran V, Kashaw SK, Agrawal RK. Recent developments and biological activities of thiazolidinone derivatives: A review. Bioorg Med Chem. 2012 Jun;20(11):3378–95.
22. Silverberg LJ, Moyer QJ. Chemistry of 1,3-thiazin-4-ones and their derivatives, 1995 - mid-2018. Arkivoc. 2019 Jun 16;2019(1):139–227.
23. Robl JA, Sun C-Q, Stevenson J, Ryono DE, Simpkins LM, Cimarusti MP, et al. Dual Metalloprotease Inhibitors: Mercaptoacetyl-Based Fused Heterocyclic Dipeptide Mimetics as Inhibitors of Angiotensin-Converting Enzyme and Neutral Endopeptidase. J Med Chem. 1997 May 1;40(11):1570–7.
24. Kouznetsov V, Rodríguez W, Stashenko E, Ochoa C, Vega C, Rolón M, et al. Transformation of schiff bases derived from alpha-naphthaldehyde. Synthesis, spectral data and biological activity of new-3-aryl-2-(α-naphtyl)-4-thiazolidinones and N-aryl-N-[1-(α-naphthyl)but-3-enyl]amines. J Heterocycl Chem. 2004;41(6):995–9.
25. Pizzo C, Saiz C, Talevi A, Gavernet L, Palestro P, Bellera C, et al. Synthesis of 2-Hydrazolyl-4-Thiazolidinones Based on Multicomponent Reactions and Biological Evaluation Against Trypanosoma Cruzi. Chem Biol Drug Des. 2011;77(3):166–72.
26. Liporagi-Lopes L, Sobhi HF, Silverberg LJ, Cordero RJB, Casadevall A. Antifungal activity of 2,3-diphenyl-2,3-dihydro-1,3-thiaza-4-ones against two human pathogenic fungi. Microbiology; 2020 Jun. Available from: http://biorxiv.org/lookup/doi/10.1101/2020.06.27.175711
27. Wirtz E, Clayton C. Inducible gene expression in trypanosomes mediated by a prokaryotic repressor. Science. 1995 May 26;268(5214):1179–83.
28. Wirtz E, Hoek M, Cross GA. Regulated processive transcription of chromatin by T7 RNA polymerase in *Trypanosoma brucei*. Nucleic Acids Res. 1998 Oct 15;26(20):4626–34.
29. DiMaio J, Ruthel G, Cannon JJ, Malfara MF, Povelones ML. The single mitochondrion of the kinetoplastid parasite *Crithidia fasciculata* is a dynamic network. López Lluch G, editor. PLoS One. 2018 Dec 28;13(12):e0202711.

30. Ochsenreiter T, Anderson S, Wood ZA, Hajduk SL. Alternative RNA Editing Produces a Novel Protein Involved in Mitochondrial DNA Maintenance in Trypanosomes. Mol Cell Biol. 2008 Sep 15;28(18):5595–604.
31. Zhao Z, Lindsay ME, Roy Chowdhury A, Robinson DR, Englund PT. p166, a link between the trypanosome mitochondrial DNA and flagellum, mediates genome segregation. EMBO J. 2008 Jan 9;27(1):143–54.
32. Klingbeil MM, Motyka SA, Englund PT. Multiple Mitochondrial DNA Polymerases in *Trypanosoma brucei*. Mol Cell. 2002 Jul;10(1):175–86.
33. Kurasawa Y, Hu H, Zhou Q, Li Z. The trypanosome-specific protein CIF3 cooperates with the CIF1 protein to promote cytokinesis in *Trypanosoma brucei*. J Biol Chem. 2018 Jun 29;293(26):10275–86.
34. Zhou Q, Gu J, Lun Z-R, Ayala FJ, Li Z. Two distinct cytokinesis pathways drive trypanosome cell division initiation from opposite cell ends. Proc Natl Acad Sci. 2016 Mar 22;113(12):3287–92.
35. Richards TA, Cavalier-Smith T. Myosin domain evolution and the primary divergence of eukaryotes. Nature. 2005 Aug;436(7054):1113–8.
36. Foth BJ, Goedecke MC, Soldati D. New insights into myosin evolution and classification. Proc Natl Acad Sci. 2006 Mar 7;103(10):3681–6.
37. Thomas JA, Baker N, Hutchinson S, Dominicus C, Trenaman A, Glover L, et al. Insights into antitrypanosomal drug mode-of-action from cytology-based profiling. Clos J, editor. PLoS Negl Trop Dis. 2018 Nov 26;12(11):e0006980.
38. Hammarton TC. Cell cycle regulation in *Trypanosoma brucei*. Mol Biochem Parasitol. 2007 May;153(1–4):1–8.
39. Li Z. Regulation of the cell division cycle in *Trypanosoma brucei*. Eukaryot Cell. 2012 Oct;11(10):1180–90.
40. Hammarton TC. Who Needs a Contractile Actomyosin Ring? The Plethora of Alternative Ways to Divide a Protozoan Parasite. Front Cell Infect Microbiol. 2019 Nov 21; 9.
41. Campbell PC, de Graffenried CL. Alternate histories of cytokinesis: lessons from the trypanosomatids. Mol Biol Cell. 2020 Nov 15;31(24):2631–9.
42. Benz C, Clucas C, Mottram JC, Hammarton TC. Cytokinesis in Bloodstream Stage *Trypanosoma brucei* Requires a Family of Katanins and Spastin. PLoS One. 2012 Jan 18;7(1):e30367.
43. Casanova M, Crobu L, Blaineau C, Bourgeois N, Bastien P, Pagès M. Microtubule-severing proteins are involved in flagellar length control and mitosis in Trypanosomatids. Mol Microbiol. 2009;71(6):1353–70.
44. Ralston KS, Lerner AG, Diener DR, Hill KL. Flagellar Motility Contributes to Cytokinesis in *Trypanosoma brucei* and Is Modulated by an Evolutionarily Conserved Dynein Regulatory System. Eukaryot Cell. 2006 Apr;5(4):696–711.
45. Broadhead R, Dawe HR, Farr H, Griffiths S, Hart SR, Portman N, et al. Flagellar motility is required for the viability of the bloodstream trypanosome. Nature. 2006 Mar 9;440(7081):224–7.
46. Chanez AL, Hehl AB, Engstler M, Schneider A. Ablation of the single dynamin of T. brucei blocks mitochondrial fission and endocytosis and leads to a precise cytokinesis arrest. J Cell Sci. 2006;119(14):2968–74.
47. Morgan GW, Goulding D, Field MC. The Single Dynamin-like Protein of *Trypanosoma brucei* Regulates Mitochondrial Division and Is Not Required for Endocytosis. J Biol Chem. 2004;279(11):10692–701.

48. Benz C, Stříbrná E, Hashimi H, Lukeš J. Dynamin-like proteins in *Trypanosoma brucei*: A division of labour between two paralogs? Mata J, editor. PLoS One. 2017;12(5):e0177200-19.
49. Allen CL, Goulding D, Field MC. Clathrin-mediated endocytosis is essential in *Trypanosoma brucei*. EMBO J. 2003;22(19):4991–5002.
50. Carter M, Gomez S, Gritz S, Larson S, Silva-Herzog E, Kim H-S, et al. A *Trypanosoma brucei* ORFeome-Based Gain-of-Function Library Identifies Genes That Promote Survival during Melarsoprol Treatment. Phillips M, editor. mSphere. 2020 Oct 7;5(5):e00769-20.
51. Baker N, Alsford S, Horn D. Genome-wide RNAi screens in African trypanosomes identify the nifurtimox activator NTR and the eflornithine transporter AAT6. Mol Biochem Parasitol. 2011 Mar;176(1):55–7.

Supplementary figures

Blank

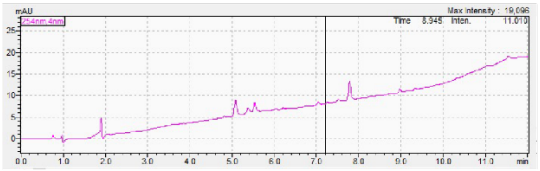

Compound 1

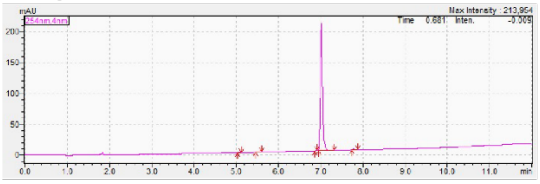

Peak#	Ret. Time	Area%
1	5.077	0.297
2	5.525	0.273
3	6.901	0.010
4	7.019	98.876
5	7.776	0.545
Total		100.000

Compound 2

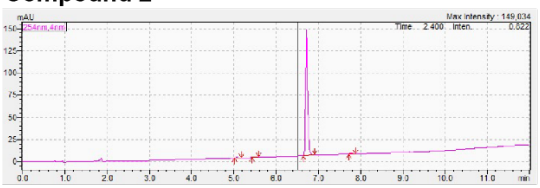

Peak#	Ret. Time	Area%
1	5.067	0.624
2	5.515	0.423
3	6.720	97.971
4	7.765	0.982
Total		100.000

Compound 3

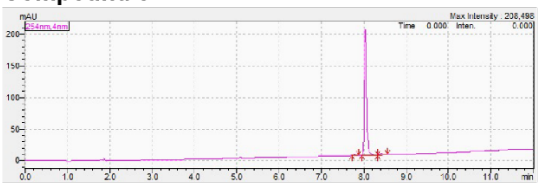

Peak#	Ret. Time	Area%
1	7.776	0.616
2	8.032	98.215
3	8.416	1.169
Total		100.000

Compound 4

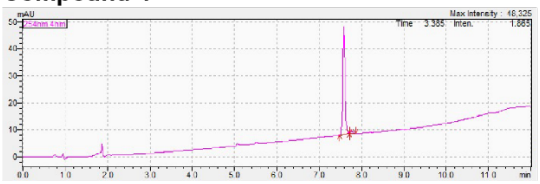

Peak#	Ret. Time	Area%
1	7.584	97.424
2	7.776	2.576
Total		100.000

Compound 5

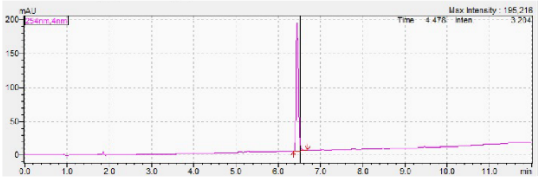

Peak#	Ret. Time	Area%
1	6.443	100.000
Total		100.000

Compound 6

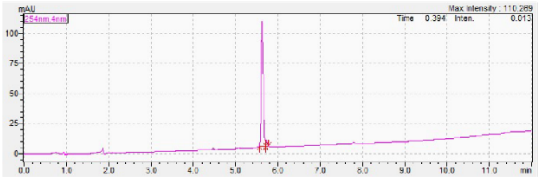

Peak#	Ret. Time	Area%
1	5.621	95.802
2	5.728	4.198
Total		100.000

Figure S1. HPLC and LC-MS analysis for estimation of compound purity. Chromatograms for each compound are shown. Tables on the right indicate the area under the curve for each peak, with the major peak indicated by a red arrow. These values were used to calculate the percent purity for each compound.

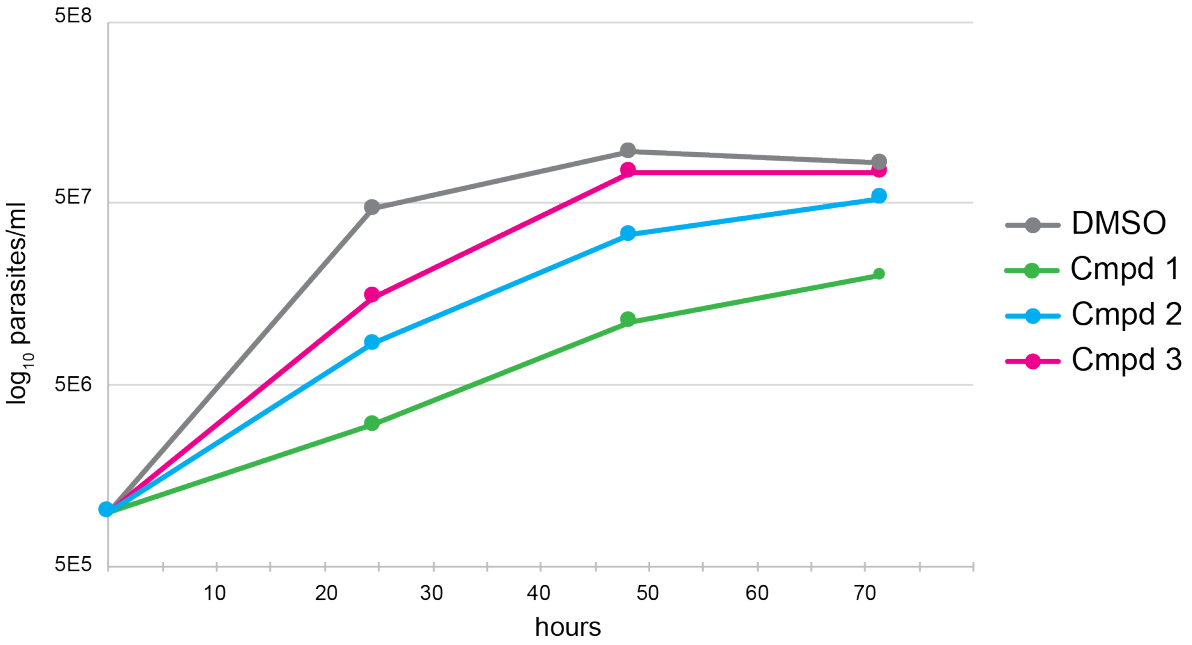

Figure S2. The effect of 2,3-diphenyl-2,3-dihydro-4*H*-1,3-thiaza-4-ones on growth of *C. fasciculata* CfC1 cells modified to express mitochondrial GFP (mitoGFP). Parasites were grown in the presence of 50 µg/ml of each compound, or a DMSO vehicle control, for 72 h.

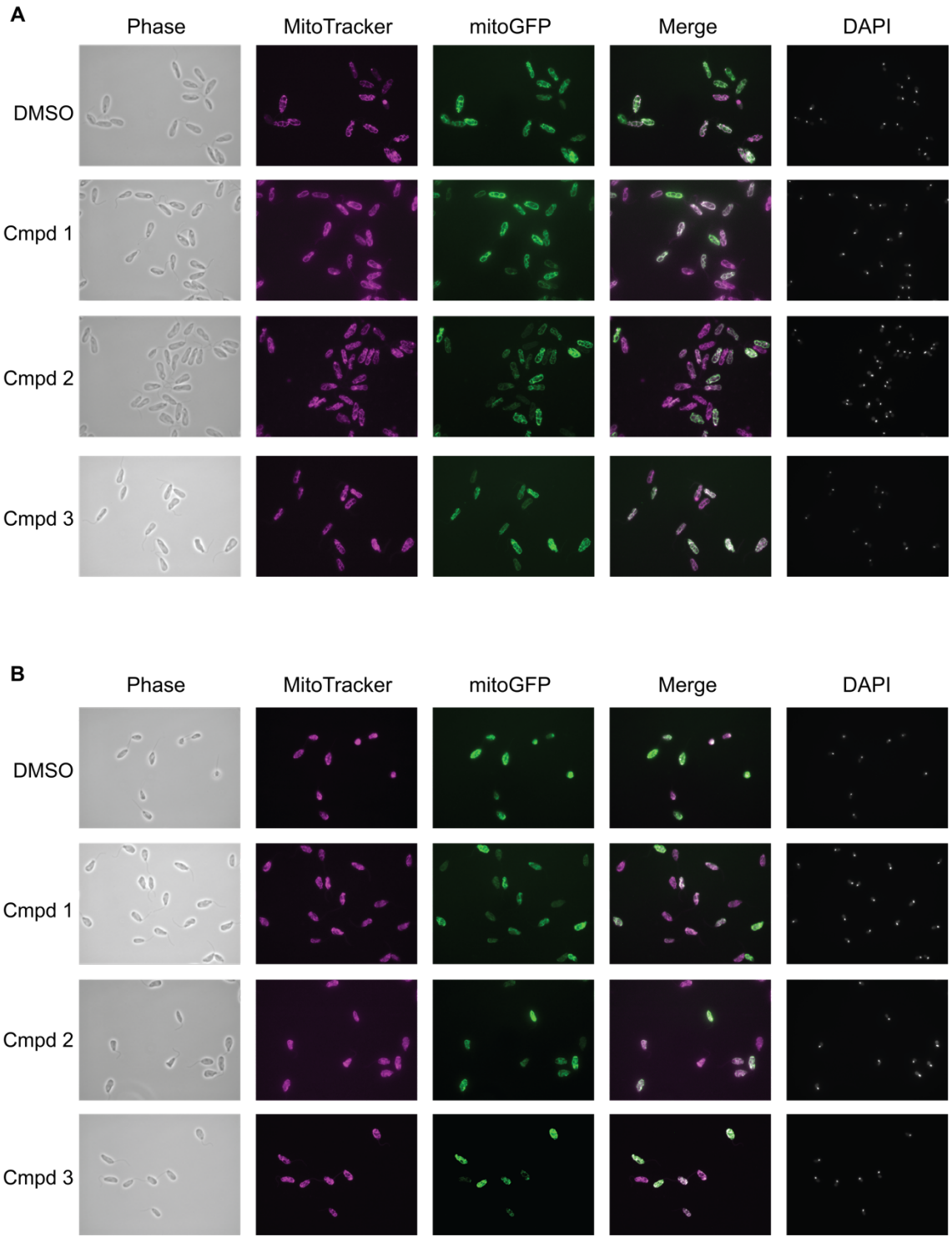

Figure S3. The effect of 2,3-diphenyl-2,3-dihydro-4*H*-1,3-thiaza-4-ones on morphology of *C. fasciculata* cells modified to express mitochondrial GFP (mitoGFP). Parasites were grown in the presence of 50 µg/ml of each compound, or a DMSO vehicle control, for (**A**) 24 h or (**B**) 48 h. Live cells were stained with MitoTracker Red, fixed, stained with DAPI, and imaged by fluorescence microscopy. Merged images were created in ImageJ.

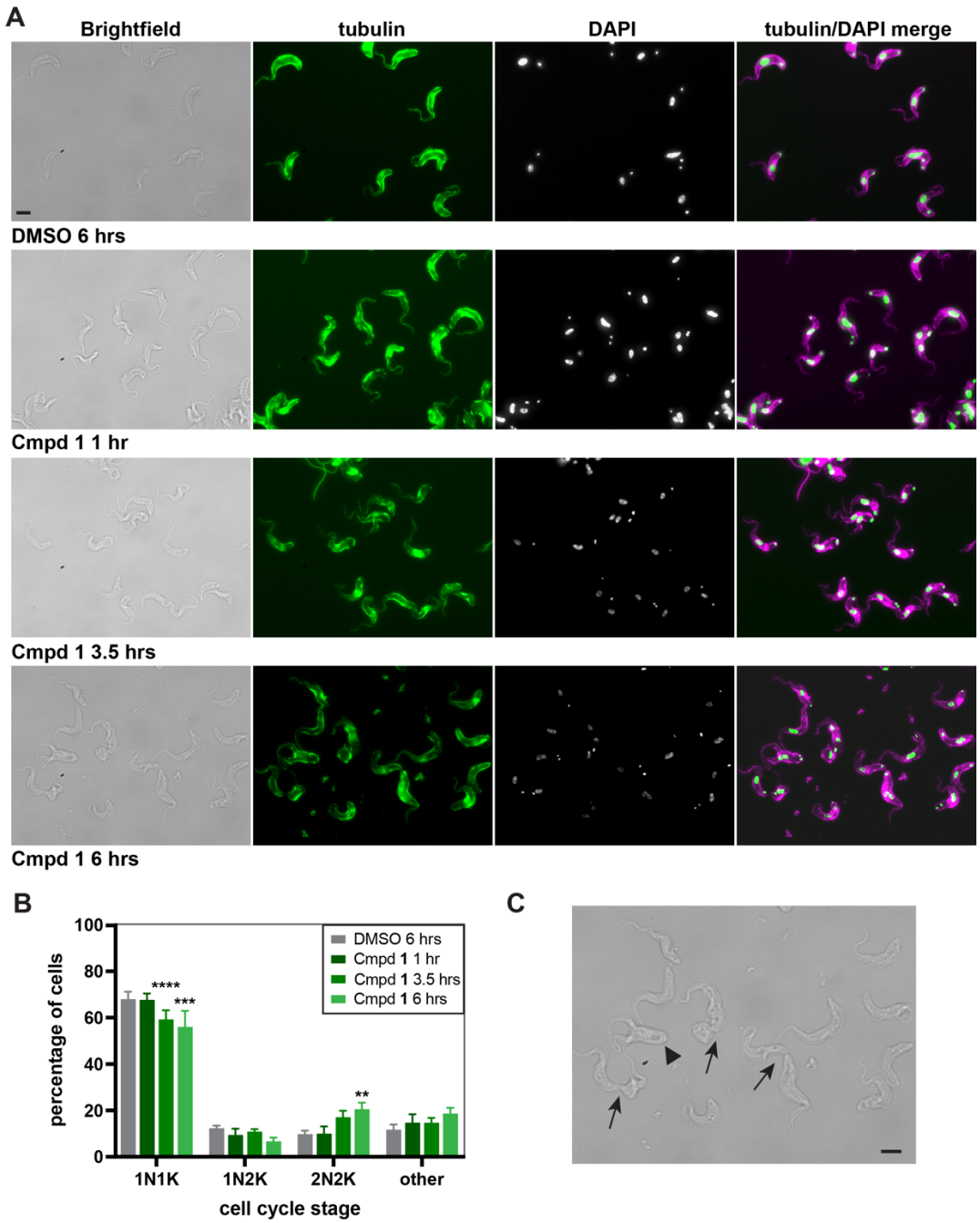

Figure S4. Effects of compound **1** on BSF *T. brucei*. (**A**) BSF *T. brucei* strain 90-13 were cultured in the presence of vehicle (DMSO) or compound **1** for 1, 3.5, or 6 hours, then subjected to immunofluorescence with an anti-alpha tubulin antibody and DAPI staining. Tubulin staining is shown in green in single channel images and magenta in merged images. (**B**) Quantitation of cell cycle stages in BSF cells treated with compound **1**. The mean of three replicates is shown (n=100-200 cells per sample per replicate). Error bars indicate standard deviation. Asterisks indicate significant differences in treated samples compared to the DMSO control and the corresponding time point, although only the latest DMSO time point is shown on the graph. **P<0.01; ***P<0.005; ****P<0.0001. (**C**) An enlargement of one of the fields shown in (**A**), with arrows/arrowheads indicating pre-abscission cells. The arrowhead indicates a cell in mid-furrow ingression, while arrows indicate cells in the final stages of pre-abscission that remain connected by a cytoplasmic bridge. Scale bars are 5 μm.

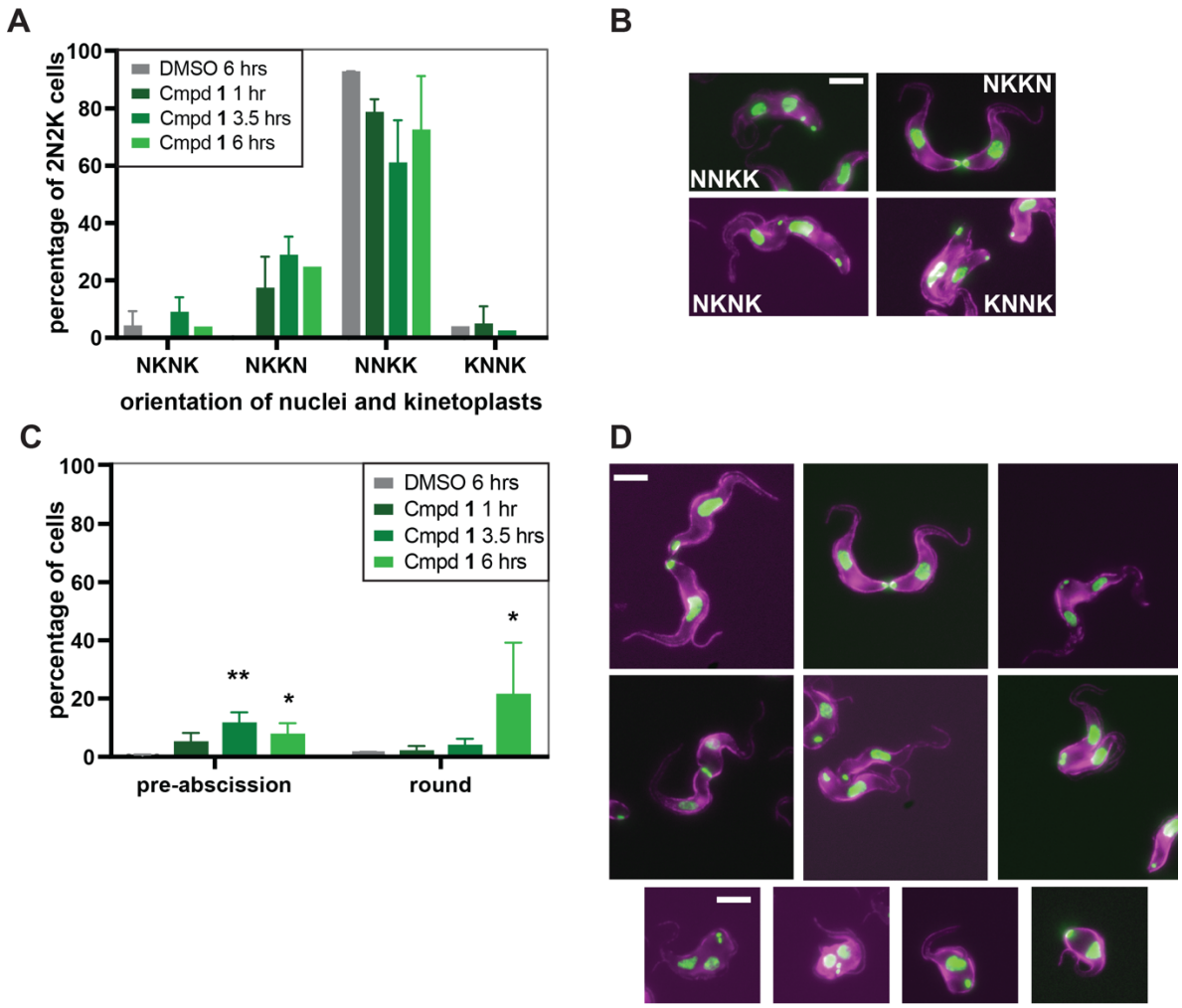

Figure S5. Compound **1**-treated BSF *T. brucei* cells display a pre-abscission arrest. (**A**) Quantitation of 2N2K cells according to configuration of nuclei (N) and kinetoplasts (K). Typically, most 2N2K BSF cells are in the NNKK configuration. Bars show the mean of two replicates. For each replicate, n=100-200 cells per sample. Error bars represent standard deviation. (**B**) Examples of cells with different arrangements of nuclei and kinetoplasts as quantitated in part (**A**). (**C**) Quantitation of pre-abscission and cells with a round morphology in BSF cultures treated with compound **1** for the indicated times. For this study, cells were counted as "pre-abscission" if they were in mid to late stages of cleavage furrow ingression with two clearly defined daughter anterior ends. The mean of three replicates is shown. Error bars show standard deviation. Asterisks indicate significance as determined by one-way no matching ANOVA with Sidak correction. * $P<0.05$, ** $P<0.1$. (**D**) Examples of treated BSF cells in pre-abscission (mid to late cleavage furrow ingression, first two rows) or what look like intermediate forms between pre-abscission and round (third row). Scale bars are 5 μm.